Numerical Model for Underground Hydrogen Storage in Cased Boreholes

Antoine Bachand[1](✉), Bernard Doyon[2], Robert Schulz[3], Ralph Rudd[4], and Jasmin Raymond[1]

[1] Institut National de la Recherche Scientifique (INRS), Québec City, Canada
antoinebachand@outlook.com
[2] Centre d'Études Nordiques (CEN), Québec City, Canada
[3] Institut de recherche d'Hydro-Québec, Québec City, Canada
[4] Department of Engineering, Reykjavik University, Québec City, Canada

Abstract. The decrease in generation costs of renewable energy, combined with advances in electrolyser technologies, suggest that green hydrogen production may be a viable option in the ongoing energy transition. Yet, a green hydrogen economy requires not only production solutions but also storage options, which prove to be challenging. An underexplored solution is the underground storage of hydrogen gas (H_2) in cased boreholes or shafts. Its integration would bring versatility in the implementation, and large applicability since it does not require a particular geological context. The objective of this paper is to evaluate the technical viability of this new storage technology. Accurate prediction of temperature and pressure variations is essential for design, materials selection and safety reasons. This work uses numerical models based on the mass and energy conservation equations to simulate hydrogen storage operations in cased boreholes. The study shows that the heat transfer at the cavity walls strongly affects temperature and pressure variations. This effect is accentuated by a borehole's geometry providing significant contact area. Thus, such technology mitigates extreme pressure and temperature variations and yields a higher hydrogen density than conventional caverns for a given pressure constraint. Results show that with a radius of 0.2 m, a hydrogen density of 30 kg m^{-3} can be attained at a maximum pressure of 50 MPa. The response of the system in terms of maximum temperature and pressure is relatively linear with an injection over 4 h but quickly becomes non-linear with a shorter injection time. The optimization of the initial storage conditions appears essential to minimize the cooling cost and maximize the storage mass.

Keywords: Energy storage · Renewable energy · Thermodynamics · Cased well · Heat transfer

1 Introduction

1.1 Context

As an energy vector, green hydrogen has received increasing attention in recent years as an attempt to overcome the intermittency of renewable energy [1]. Indeed, energy

P. Schossig et al. (Eds.): IRES 2022, AHE 16, pp. 14–28, 2023.
https://doi.org/10.2991/978-94-6463-156-2_3

like solar and wind exhibit a mismatch between the fluctuating power generation and the demand [2]. Power to gas technology has the potential to sustainably alleviate this imbalance with the chemical storage of electricity such as hydrogen, ammonia, or synthetic fuel [2]. In addition, green hydrogen is proving to be an attractive route for the decarbonization of the transportation and industrial sector. Ships [3], remote trains[4], long distance trucks [5], steal production [6], fertiliser [7, 8], and high temperature industrial heat [9] are just few examples of hard to abate sectors that can be leveraged to achieve ambitious climate goals [10].

With the conjuncture of electrolyzers commercialization and declining costs of renewable energy [11], cost forecasting analysis [12–14] suggests that large-scale green hydrogen production can be a viable component of the energy transition.

However, a green hydrogen economy requires not only production solutions but also storage options, which prove to be challenging. Innovations in liquid organic hydrogen carrier (LOHC) [15, 16] and metal hydride (MH) [17, 18] technologies are promising, although they are still constrained by technical and economic bottlenecks [19, 20]. As for conventional hydrogen tanks (2–15 m^3 [21]), they still have some problems that affect performance and cost effectiveness, such as gas leaks, hazards of hydrogen jet diffusion flame [22], temperature rise in the fast-filling process [23–25], embrittlement and fatigue crack growth [26].

On a large scale (30,000–1,000,000 m^3 [27]), storage solutions are limited to underground hydrogen storage (UHS) in geological environments such as salt caverns [28–30], aquifers [31, 32] and depleted oil and gas reservoirs [33]. However, depleted gas reservoirs and aquifers present challenges with leakage management and environmental impacts [27]. Salt caverns appear to be a tighter environment and the most economic alternative [34, 35]. Models were even established recently for the construction of caverns at depths of more than 2,000 m [36] and in the deep sea [37–39]. However, occurrence and quality of salt formation is specific to certain regions. In the province of Quebec, salt formations are only occurring in the Magdalen Basin in the Gulf of St. Lawrence [40, 41].

An alternative and still relatively underexplored solution is the storage of hydrogen gas in cased boreholes or shafts (Fig. 1). It has potential to drive a rapid deployment of UHS, especially for industrial purposes. Indeed, its integration would bring versatility in the implementation, and better reproducibility since it does not require a particular geological context to install the storage infrastructure.

1.2 Formulation of the Problem

The development of this type of storage technology is facing several barriers such as technical and safety limitations, legal barriers, cost effectiveness, conflicts of interest and social acceptance [42]. The present study focuses on technical and safety limitations only and makes certain assumptions.

First, the study assumes that the well casing can operate at a maximum pressure of between 50 and 60 MPa; indeed, this type of pressure is common in oil and gas wells [43, 44].

Second, hydrogen resistant structural materials have attracted a lot of research interest lately notably for pipeline application [45, 46] and hydrogen conversion of underground

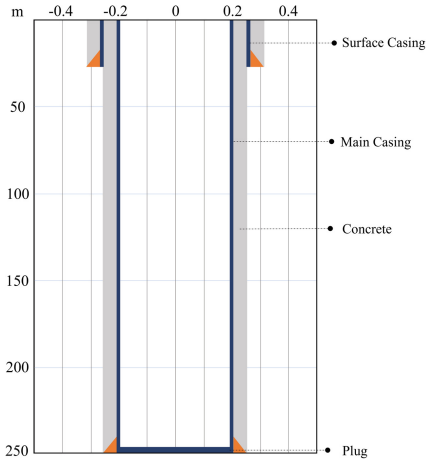

Fig. 1. Design of a hydrogen storage infrastructure in a cased borehole.

natural gas storage [47]. However, these applications are not subject to a pressure regime comparable to the one targeted by the cased borehole storage technology. Therefore, the study assumes a careful selection of well components, including casing, tubing, cement and plug. For example, high-strength steel can be severely affected by hydrogen embrittlement [48]. Hence, the selection of appropriate materials will require consideration of hydrogen blistering, hydrogen-induced cracking, embrittlement, cement degradation, elastomer failure and microbial casing corrosion [48]. The latter is however greatly reduced as the system is closed and the hydrogen is not in direct contact with a geological reservoir.

Temperature and pressure predictions can ensure the integrity of these components which are indeed sensitive to operating conditions. Such predictions are also required for the selection of the storage volume and the injection temperature. Thus, the present study addresses the evaluation of pressure and temperature variations during the operation cycle of hydrogen storage in a cased borehole.

Kushnir et al. [49] developed a numerical model for temperature and pressure variations in CAES cavern on the basis of mass and energy conservation equations coupled with the conduction equation of the surrounding rocks. In their paper, the air properties were based on a simplified thermodynamic model that appeared adequate for the targeted pressure variations (of the order of 2 MPa). However, in order to evaluate the technical viability of the technology through prediction of pressure and temperature variations, this study adapts the Kushnir et al. [49] model for hydrogen and utilizes an exact gas model for thermodynamic properties that was found to be robust to cover a wide range of pressure variation.

Table 1. Geometrical parameters

Input parameter	Case 1 (Borehole)	Case 2 (Shaft-Cavern)
Radius (m)	0.2	1
Length (m)	250	10
Volume (m^3)	31.43	31.43

2 Methodology

2.1 Numerical Model

The temperature and pressure variation during hydrogen storage operation can be calculated using the numerical model of Kushnir et al. [49] (initially written for air storage), with modifications considering the thermodynamic properties of hydrogen. Thus, the mass and energy conservation equations, subject to the generalized gas equation, are:

$$V\frac{d\rho}{dt} = (F_i + F_e)\dot{m}_c \tag{1}$$

$$V\rho c_{\mathrm{v}}\frac{dT}{dt} = F_i\dot{m}_c(h_i - h) + ([F_i + F_e]\dot{m}_c)\left(ZRT - \rho\frac{\partial u}{\partial \rho}\bigg|_T\right) + \dot{Q} \tag{2}$$

$$p = Z\rho RT \tag{3}$$

In the above equations, V (m^3) is the cavity volume, ρ (kg m^{-3}) is the gas density, F_i and F_e are respectively the injection and extraction functions (dimensionless and periodic), $\dot{m}_c$ (kg s^{-1}) is the gas mass flow rate, c_{v} (J kg ^{1} K^{-1}) is the constant volume specific heat, T (K) is the gas temperature, t (s) is the time, h (J) is the specific enthalpy, h_i (J) is the injected specific enthalpy, u (J kg^{-1}) is the specific internal energy, Z (−) is the gas compressibility factor, R (J kg^{-1} K^{-1}) is the specific gas constant, $\dot{Q}$ (W) is the heat transfer rate across the cavern walls and p (Pa) is the gas pressure.

The heat losses can be expressed in Eq. (4) by the heat transfer coefficient, h_c (W m^{-2} K^{-1}), the total surface of the cavity, A_c (m^2) and the rock wall temperature, T_{R_w} (K).

$$\dot{Q} = h_c A_c (T_{R_w} - T) \tag{4}$$

The temperature at the cavity wall (the term T_{R_w} in Eq. (4) varies with time and is obtained by solving Eq. (5), which gives the temperature in the rock (T_{R}) as a function of time and distance r (m) from the center of the cylindrical cavity. In the later, ρ_R (kg m^{-3}) is the rock density, k_R (W m^{-1} K^{-1}) is the thermal conductivity of rock and c_{pR} (J Kg^{-1} K^{-1}) is the constant pressure specific heat capacity of rock.

$$\rho_R c_{pR}\frac{dT_R}{dt} = \frac{1}{r}\frac{\partial}{\partial r}\left(k_R r\frac{\partial T_{\mathrm{R}}}{\partial \mathrm{r}}\right) \tag{5}$$

Table 2. Operating parameters

Input parameter	Values
Injection temperature (°C)	50
Initial temperature (°C)	30
Initial pressure (kPa)	101.3
Mass rate (kg s^{-1})	0.0944
Target mass (kg)	935

Equations (1), (2) and (5) can be transformed into a system of coupled differential equations with initial conditions. In order to do this, Eq. (5) must be discretized with appropriate boundary conditions (see Kushnir et al. [49] for details). The solution for the time evolution of temperature in the cavity is obtain by numerically integrating the system of differential equations thus formed. We used a non-stiff solver for the injection phase and a stiff solver for the discharge and storage period. With the help of thermodynamic properties relationships, the enthalpies (h and h_i), the specific heat (c_v) and the partial derivative of internal energy with respect to density ($\rho \frac{\partial u}{\partial \rho}\Big|_T$) are calculated at each time step of the numerical integration scheme using the corresponding pressure and density with Eq. (3). Furthermore, we used the specific hydrogen compressibility model of Lemmon et al. [50] to calculate, at each time step, the compressibility factor (Z) (and its derivatives appearing in the thermodynamic properties). The equations for the thermodynamic properties relationships, the compressibility factor for hydrogen and its derivatives are not given in this paper.

The temperature obtained numerically with our code was validated by comparing it with the analytical and semi analytical solutions for adiabatic and perfect conduction scenarios given in Kushnir et al. [49]. The compressibility factor, enthalpy and specific heat calculated with our code at different pressure and temperature was validated with published data for hydrogen [51].

2.2 Simulations

2.2.1 Geometry

In order to compare the thermodynamic responses, the study considered not only the cased borehole geometry but also a more studied geometry that is similar to an abandoned mine shaft or cylindrical mine cavern [35, 49, 52, 53]. Thus, the two geometry scenarios are presented in Table 1 and since the storage volume remains constant between both cases, it allows to maintain the same injection rate.

2.2.2 Operating Parameters

Regarding the operating parameters, the study considers a 24-h storage cycle with a period of injection, storage and withdrawal. The mass flow rate used is equivalent to the hydrogen production of a Silyzer 300 electrolyzer of 17.5 MW (340 kg h^{-1}) developed

Table 3. Thermal properties

Input parameter	Values
Thermal conductivity of rock (W m^{-1} K^{-1})	2.6
Specific heat capacity of rock (J Kg^{-1} K^{-1})	820
Density of rock (kg m^{-3})	2200
Diffusivity of rock (mm^2 s^{-1})	1.44
Effusivity of rock (W $s^{0.5}$ m^{-2} K^{-1})	2165
Heat transfer coefficient (W m^{-2} K^{-1})	30

by Siemens Energy [54]. The target storage mass is 935 kg or 29.75 kg m^{-3} and involves an injection time of 2.75 h. Variation of the injection speed has also been investigated. Indeed, the study asses the influence of the parameters of injection speed and injection temperature to maximize the storage mass by optimization. Specifically, the sensitivity analysis was split between factors associated with the operation of the infrastructure and those associated with the site. The operation parameters are summarized in Table 2.

2.2.3 Site-Related Parameters

Site-related input parameters are thermal properties of the rock and are listed in Table 3. The thermal conductivity, heat capacity and density given are those associated with a shale rock [55], which is typical of the St Lawrence Lowlands in Quebec. Since the thermal conductivity and heat capacity vary with mineralogy (mostly quartz content), porosity and anisotropy of the rock [56], a sensitivity analysis was conducted to evaluate the impact of the rock thermal properties. Thermal conductivity of rocks usually ranges between 0.40 and 7.00 W m^{-1} K^{-1} [56].

$$\alpha_R = \frac{k_R}{\rho_R c_{pR}} \tag{6}$$

$$e_R = \sqrt{k_R \rho_R c_{pR}} \tag{7}$$

The thermal diffusivity of rock, α_R (m^2 s^{-1}) is given by Eq. (6). It expresses the speed at which a material responds to a change in temperature [56] and is widely used in the literature. In contrast, Kushnir et al. [49] uses the thermal effusivity of rock, e_R (W $s^{0.5}$ m^{-2} K^{-1}) which reflects the ability of a material to exchange heat with the environment, i.e., to store or dissipate heat [56]. The thermal effusivity is directly related to the thermal diffusivity, allowing a comparison of results through their relationship with Eq. (6) and Eq. (7). The sensitivity analysis on diffusivity corresponds to a thermal conductivity range of 0.8 to 4.5 W m^{-1} K^{-1}.

In Kushnir et al. [49], the heat transfer coefficient is represented by a constant value of 30 W m^{-2} K^{-1}. This assumption was suitable for the case of a cavern due to the

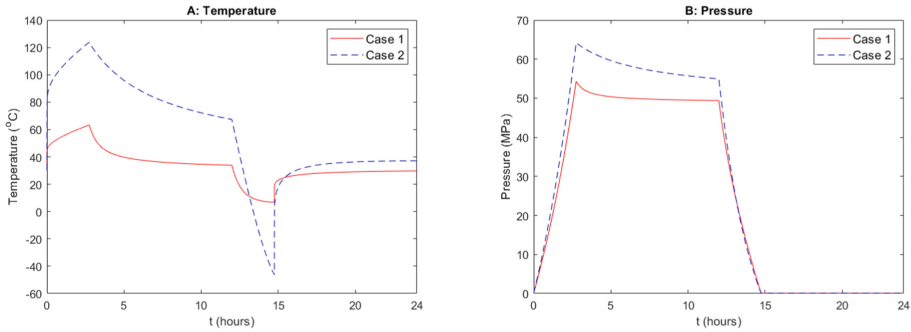

Fig. 2. Pressure and temperature evolution with a hydrogen flow rate of 340 kg/h (equivalent to the production of the 17.5 MW Silyzer electrolyzer) for different geometry cases.

successful reproduction of the operational data of the Huntorf CAES power plant. Our model allows us to use a time-dependent heat transfer coefficient. Indeed, the convective heat transfer coefficient is dependent on the properties of the gas, the shape and size of the cavity, and the temperature difference between the gas and the wall [49, 57]. In addition, turbulent gas flow due to charging or discharging of the reservoir can increase the heat transfer coefficient [57].

Thus, an estimation or laboratory measurement of the heat transfer coefficient specific to the design of hydrogen storage in cased borehole at high pressure regime would be beneficial. In the present study we have conducted a sensitivity analysis of this factor using a base value of 30 W m^{-2} K^{-1}.

3 Results

3.1 Storage Cycle and Geometry

The temperature and pressure variations in the cavity were studied for a 24 h operational cycle where the extraction takes place at 12:00 after 9 h and 15 min of storage. In addition, the extraction mass flow rate is equivalent to the injection flow rate. Also, in addition to addressing the cased borehole geometry of Case 1, the study considers a second geometry (Case 2) which reflects an increase in borehole radius from 0.2 to 1 m with an infrastructure analogous to a mine shaft or abandoned mine cavern allowing a larger scale storage.

Figure 2 shows that for Case 1 (cased borehole), the operating parameters of Table 2 generates a slight pressure peak reaching 54 MPa and the temperature remains below 65 °C. In addition, the extraction generates a temperature that remains above the freezing point in the borehole (7 °C). As for case two, it exhibits a higher pressure and temperature variation with a range of 123 to −47 °C and a significant pressure peak of 64.5 MPa.

This discrepancy between the geometry scenarios is due to the difference in contact area. Indeed, a high surface contact accentuates the heat transfer between the hydrogen and the rock limiting extreme fluctuations of temperature and pressure.

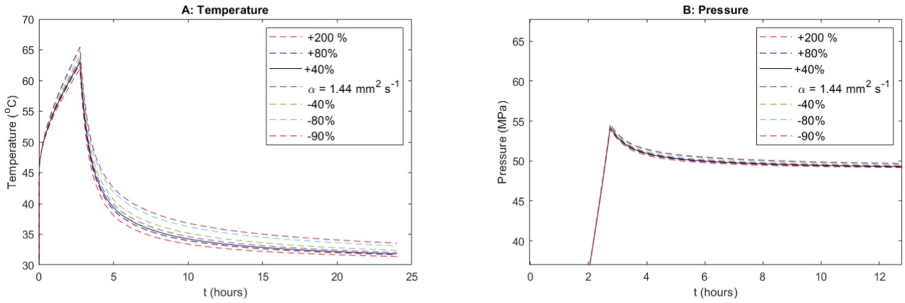

Fig. 3. Sensitivity analysis of the heat transfer coefficient on the cased borehole design (Case 1).

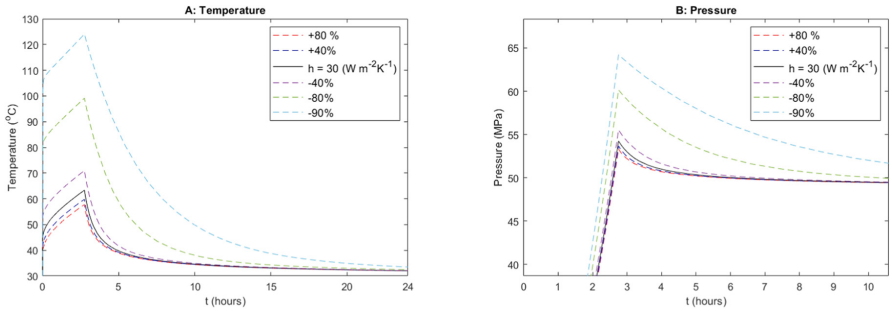

Fig. 4. Sensitivity of the heat transfer coefficient on the cased borehole design (Case 1).

3.2 Thermal Diffusivity

Figure 3 presents a sensitivity analysis on the rock thermal diffusivity for Case 1. It allows to assess the impact of the various rock types and to understand the impact of different heat transfer processes. The decrease of 90% to an increase of 200% on thermal diffusivity with respect to the base case value of 1.44 $mm^2\ s^{-1}$ shows a narrow range of temperature and pressure variations. The thermal conductivity mostly controls heat diffusion in the rock. As for the gas temperature, it is related to the heat loss which depends on the contact surface but also on the temperature difference between gas and rock. With this geometry, even a low thermal conductivity ensures that the heat propagates in the rock and therefore the wall remains cooler than the gas, thus allowing efficient heat exchange.

3.3 Heat Transfer Coefficient

Figure 4 shows a sensitivity analysis on the heat transfer coefficient for Case 1 since the specific geometry and pressure regime requires to estimate this parameter. The analysis reflects an increase and decrease of the heat transfer coefficient up to 90%. A more significant increase of the parameter was not undertaken since a heat transfer coefficient that tends to infinity simply generates a temperature that converges to the rock's initial temperature.

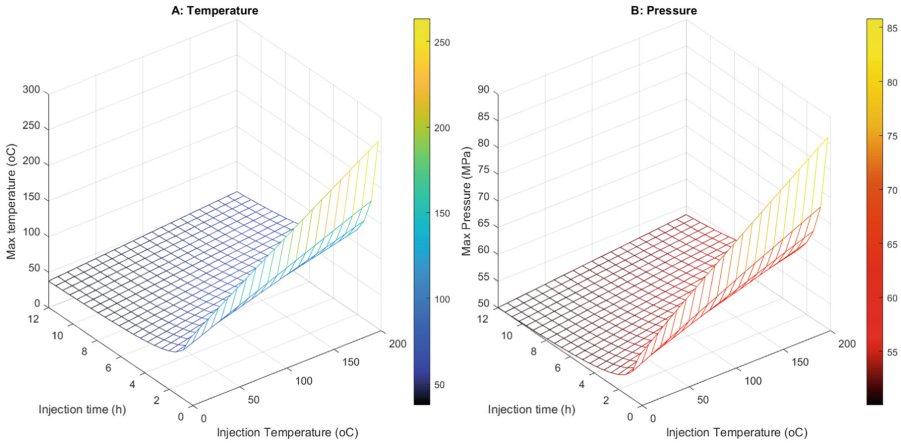

Fig. 5. Sensitivity of the operating parameters with the cased borehole design (Case 1) and the thermal properties of Table 3.

Thus, the interest lies mainly in the decrease of the heat transfer coefficient. A decline of 90% from 30 to 3 W m^{-2} K^{-1} generates a significant pressure and temperature peak and a deeper decrease of the coefficient leads to an exponential effect.

3.4 Operating Conditions

Figure 5 investigates the impact of operational factors, i.e., injection rate and injection temperature, on the maximum temperature and pressure achieved in the cycle with the cased borehole geometry (Case 1). It shows that with over 4 h of injection time, even an injection temperature of 200 °C results in a maximum pressure of less than 60 MPa and a temperature of less than 90 °C. As for the previous injection time of 2.75 h, a pressure of 60 MPa is reached at an injection temperature of 160 °C. Moreover, it appears that the response of the system is quite linear for this range of injection speed (over 4 h). On the other hand, beyond a certain speed, the maximum temperature and pressure reached during the charging process rises considerably.

A compelling comparison is made between these results and the geometry of Case 2 (Fig. 6), which reflects a design intended for larger-scale storage, analogous to a mine shaft or abandoned mine cavern. This decrease in contact area to volume ratio generates a system response that is nonlinear across the domain and an optimization method is desired to maximize storage mass and minimize cooling costs while meeting design constraints.

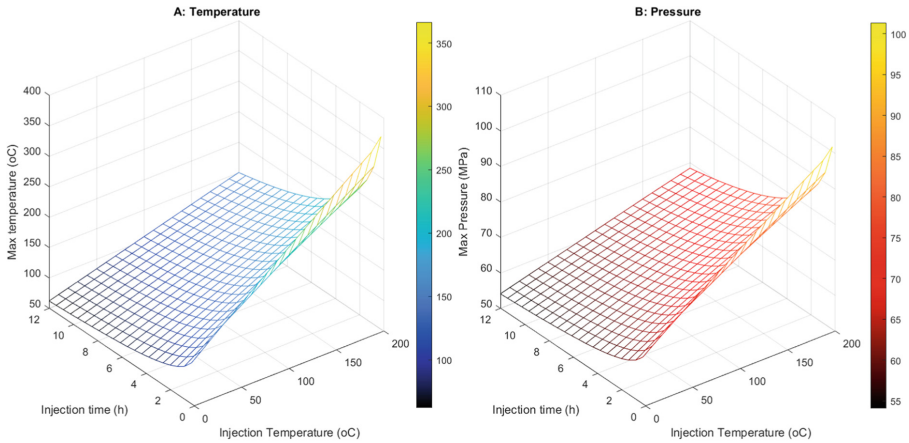

Fig. 6. Sensitivity of the operating parameters on Case 2 with the thermal properties of Table 3.

4 Discussion and Conclusions

In summary, the geometry of the cased borehole concept offers an advantage over a large diameter cavern or shaft design. While a high surface area to volume ratio increases the mass flow rate and likelihood of leakage [52, 53], it also enhances heat exchanges and thereby limits extreme temperature and pressure variations. Indeed, this greater heat transfer rate with a smaller diameter maximizes the storage mass for a given pressure constraint while minimizing the risk of thermal shock between injection and extraction stages.

Thus, the system may even be analogous to the isothermal technology developed for CAES [52–54], which aims to maintain a constant temperature in the cavity. It therefore allows higher pressures without significant temperature variation, and the input of fossil energy for gas expansion becomes unnecessary, which results in greater efficiency [59]. Indeed, in the case of borehole storage, the rock has the potential to cool and warm the gas during injection and extraction.

However, a measurement or estimation of the heat transfer coefficient for this specific application is recommended for future work. A low heat transfer coefficient would reduce the propagation of the thermal perturbation in the host rock. Interest should also be given to rock formations with high thermal diffusivity, but this does not represent a constraint to the implementation since its effect on the heat transfer is minor in comparison to the surface area or geometry. Even a low thermal diffusivity allows heat to propagate in the rock and maintains a temperature difference between the wall and the gas.

Regarding the operating parameters, for a hydrogen storage density of 30 kg m^{-3} and a radius of 0.2 m, an injection of more than 4 h can sustain an injection temperature of 200 °C with a maximum pressure below 60 MPa and a maximum temperature under 90 °C in the borehole. Indeed, the response of the system in terms of maximum temperature and pressure is relatively linear. On the other hand, the thermodynamic response of the system quickly becomes non-linear with a shorter injection time or a modification of the geometry.

Thus, an optimized operating procedure is recommended to maximize storage content and minimize maximum temperature especially in cases of fast injection and large radius infrastructures (more than 0.5 m).

Acknowledgments. This project was funded by the Natural Sciences and Engineering Research Council of Canada (NSERC). The authors also wish to acknowledge the financial support of Hydro-Québec.

Authors' Contributions. **Antoine Bachand**: Conceptualization, Data processing, Programming and Writing – original draft.

Bernard Doyon: Numerical model programming and Reviewing.

Robert Schulz: Reviewing.

Ralph Rudd: Reviewing.

Jasmin Raymond: Supervision, Reviewing and Editing.

References

1. Z. Heydarzadeh, J. Brouwer, Investigation of Southern California Natural Gas Infrastructure to Transport and Store Hydrogen to Meet Electric Demand Based on a 100% Renewable Energy Portfolio, in: 2020: p. 10. https://doi.org/10.1115/POWER2020-16044.
2. M. Bailera, P. Lisbona, B. Peña, L. Romeo, Energy Storage, Hybridization of Power-to-Gas Technology and Carbon Capture, Springer, 2020. https://doi.org/10.1007/978-3-030-46527-8.
3. Ricardo, Environmental Defense, Indonesia: fuelling the future of shipping, Report, Environmental Defense Fund, Jakarta, (2021) 68 p. https://www.globalmaritimeforum.org/content/2021/11/EDF-Zero-carbon-shipping-Indonesia-FINAL.pdf.
4. G.D. Marin, G.F. Naterer, K. Gabriel, Rail transportation by hydrogen vs. electrification – Case study for Ontario, Canada, II: Energy supply and distribution, International Journal of Hydrogen Energy. 35 (2010) 6097–6107. https://doi.org/10.1016/j.ijhydene.2010.03.095.
5. J. Lao, H. Song, C. Wang, Y. Zhou, J. Wang, Reducing atmospheric pollutant and greenhouse gas emissions of heavy duty trucks by substituting diesel with hydrogen in Beijing-Tianjin-Hebei-Shandong region, China, International Journal of Hydrogen Energy. 46 (2021) 18137–18152. https://doi.org/10.1016/j.ijhydene.2020.09.132.
6. P. Hodaly Rodríguez, Applications for large scale hydrogen production in wind parks, Master's Thesis, Universitat Politècnica de Catalunya, (2020) 95 p. http://hdl.handle.net/2117/333812.
7. Z. Cesaro, M. Ives, R. Nayak-Luke, M. Mason, R. Bañares-Alcántara, Ammonia to power: Forecasting the levelized cost of electricity from green ammonia in large-scale power plants, Applied Energy. 282 (2021) 116009. https://doi.org/10.1016/j.apenergy.2020.116009.
8. C. Smith, L. Torrente-Murciano, The potential of green ammonia for agricultural and economic development in Sierra Leone, One Earth. 4 (2021) 104–113. https://doi.org/10.1016/j.oneear.2020.12.015.
9. G. Kakoulaki, I. Kougias, N. Taylor, F. Dolci, J. Moya, A. Jäger-Waldau, Green hydrogen in Europe – A regional assessment: Substituting existing production with electrolysis powered by renewables, Energy Conversion and Management. 228 (2021) 113649. https://doi.org/10.1016/j.enconman.2020.113649.

10. M.-K. Kazi, F. Eljack, M.M. El-Halwagi, M. Haouari, Green hydrogen for industrial sector decarbonization: Costs and impacts on hydrogen economy in qatar, Computers & Chemical Engineering. 145 (2021) 107144. https://doi.org/10.1016/j.compchemeng.2020.107144.
11. IRENA, How Falling Costs Make Renewables a Cost-effective Investment, (2020). https://www.irena.org/newsroom/articles/2020/Jun/How-Falling-Costs-Make-Renewables-a-Cost-effective-Investment (accessed December 19, 2021).
12. C. Augustine, N. Blair, Storage Futures Study: Storage Technology Modeling Input Data Report, National Renewable Energy Lab. (NREL), Golden, CO (United States), 2021. https://doi.org/10.2172/1785959.
13. C.A. Hunter, M.M. Penev, E.P. Reznicek, J. Eichman, N. Rustagi, S.F. Baldwin, Techno-economic analysis of long-duration energy storage and flexible power generation technologies to support high-variable renewable energy grids, Joule. 5 (2021) 2077–2101. https://doi.org/10.1016/j.joule.2021.06.018.
14. O. Schmidt, S. Melchior, A. Hawkes, I. Staffell, Projecting the Future Levelized Cost of Electricity Storage Technologies, Joule. 3 (2019) 81–100. https://doi.org/10.1016/j.joule.2018.12.008.
15. M. Reuß, T. Grube, M. Robinius, P. Preuster, P. Wasserscheid, D. Stolten, Seasonal storage and alternative carriers: A flexible hydrogen supply chain model, Applied Energy. 200 (2017) 290–302. https://doi.org/10.1016/j.apenergy.2017.05.050.
16. M. Niermann, S. Timmerberg, S. Drünert, M. Kaltschmitt, Liquid Organic Hydrogen Carriers and alternatives for international transport of renewable hydrogen, Renewable and Sustainable Energy Reviews. 135 (2021) 110171. https://doi.org/10.1016/j.rser.2020.110171.
17. G. Han, Y. Kwon, J.B. Kim, S. Lee, J. Bae, E. Cho, B.J. Lee, S. Cho, J. Park, Development of a high-energy-density portable/mobile hydrogen energy storage system incorporating an electrolyzer, a metal hydride and a fuel cell, Applied Energy. 259 (2020) 114175. https://doi.org/10.1016/j.apenergy.2019.114175.
18. B.P. Tarasov, P.V. Fursikov, A.A. Volodin, M.S. Bocharnikov, Y.Y. Shimkus, A.M. Kashin, V.A. Yartys, S. Chidziva, S. Pasupathi, M.V. Lototskyy, Metal hydride hydrogen storage and compression systems for energy storage technologies, International Journal of Hydrogen Energy. 46 (2021) 13647–13657. https://doi.org/10.1016/j.ijhydene.2020.07.085.
19. P.C. Rao, M. Yoon, Potential Liquid-Organic Hydrogen Carrier (LOHC) Systems: A Review on Recent Progress, Energies. 13 (2020) 6040. https://doi.org/10.3390/en13226040.
20. C. Zhang, P. Song, Y. Zhang, L. Xiao, J. Hou, X. Wang, Technical and cost analysis of imported hydrogen based on MCH-TOL hydrogen storage technology, International Journal of Hydrogen Energy. (2022). https://doi.org/10.1016/j.ijhydene.2022.06.113.
21. J. Zheng, X. Liu, P. Xu, P. Liu, Y. Zhao, J. Yang, Development of high pressure gaseous hydrogen storage technologies, International Journal of Hydrogen Energy. 37 (2012) 1048–1057. https://doi.org/10.1016/j.ijhydene.2011.02.125.
22. T. Mogi, S. Horiguchi, Experimental study on the hazards of high-pressure hydrogen jet diffusion flames, Journal of Loss Prevention in the Process Industries. 22 (2009) 45–51. https://doi.org/10.1016/j.jlp.2008.08.006.
23. S. Maus, J. Hapke, C.N. Ranong, E. Wüchner, G. Friedlmeier, D. Wenger, Filling procedure for vehicles with compressed hydrogen tanks, International Journal of Hydrogen Energy. 33 (2008) 4612–4621. https://doi.org/10.1016/j.ijhydene.2008.06.052.
24. D. Melideo, D. Baraldi, M.C. Galassi, R. Ortiz Cebolla, B. Acosta Iborra, P. Moretto, CFD model performance benchmark of fast filling simulations of hydrogen tanks with pre-cooling, International Journal of Hydrogen Energy. 39 (2014) 4389–4395. https://doi.org/10.1016/j.ijhydene.2013.12.196.
25. G. Liu, Y. Qin, Y. Liu, Numerical simulation of hydrogen filling process in novel high-pressure microtube storage device, International Journal of Hydrogen Energy. 46 (2021) 36859–36871. https://doi.org/10.1016/j.ijhydene.2021.08.227.

26. T. Kanezaki, C. Narazaki, Y. Mine, S. Matsuoka, Y. Murakami, Effects of hydrogen on fatigue crack growth behavior of austenitic stainless steels, International Journal of Hydrogen Energy. 33 (2008) 2604–2619. https://doi.org/10.1016/j.ijhydene.2008.02.067.
27. D. Zivar, S. Kumar, J. Foroozesh, Underground hydrogen storage: A comprehensive review, International Journal of Hydrogen Energy. 46 (2021) 23436–23462. https://doi.org/10.1016/j.ijhydene.2020.08.138.
28. R. Tarkowski, G. Czapowski, Salt domes in Poland – Potential sites for hydrogen storage in caverns, International Journal of Hydrogen Energy. 43 (2018) 21414–21427. https://doi.org/10.1016/j.ijhydene.2018.09.212.
29. D.G. Caglayan, N. Weber, H.U. Heinrichs, J. Linßen, M. Robinius, P.A. Kukla, D. Stolten, Technical potential of salt caverns for hydrogen storage in Europe, International Journal of Hydrogen Energy. 45 (2020) 6793–6805. https://doi.org/10.1016/j.ijhydene.2019.12.161.
30. W. Liu, Z. Zhang, J. Chen, D. Jiang, F. Wu, J. Fan, Y. Li, Feasibility evaluation of large-scale underground hydrogen storage in bedded salt rocks of China: A case study in Jiangsu province, Energy. 198 (2020) 117348. https://doi.org/10.1016/j.energy.2020.117348.
31. A. Sainz-Garcia, E. Abarca, V. Rubi, F. Grandia, Assessment of feasible strategies for seasonal underground hydrogen storage in a saline aquifer, International Journal of Hydrogen Energy. 42 (2017) 16657–16666. https://doi.org/10.1016/j.ijhydene.2017.05.076.
32. N. Heinemann, M.G. Booth, R.S. Haszeldine, M. Wilkinson, J. Scafidi, K. Edlmann, Hydrogen storage in porous geological formations – onshore play opportunities in the midland valley (Scotland, UK), International Journal of Hydrogen Energy. 43 (2018) 20861–20874. https://doi.org/10.1016/j.ijhydene.2018.09.149.
33. A. Amid, D. Mignard, M. Wilkinson, Seasonal storage of hydrogen in a depleted natural gas reservoir, International Journal of Hydrogen Energy. 41 (2016) 5549–5558. https://doi.org/10.1016/j.ijhydene.2016.02.036.
34. Z. Tong, Z. Cheng, S. Tong, A review on the development of compressed air energy storage in China: Technical and economic challenges to commercialization, Renewable and Sustainable Energy Reviews. 135 (2021) 110178. https://doi.org/10.1016/j.rser.2020.110178.
35. M. AbuAisha, A. Rouabhi, J. Billiotte, F. Hadj–Hassen, Non–isothermal two–phase hydrogen transport in rock salt during cycling in underground caverns, International Journal of Hydrogen Energy. 46 (2021) 6632–6647. https://doi.org/10.1016/j.ijhydene.2020.11.152.
36. T.T. Wang, H.L. Ma, X.L. Shi, C.H. Yang, N. Zhang, J.L. Li, S.L. Ding, J.J.K. Daemen, Salt cavern gas storage in an ultra-deep formation in Hubei, China, International Journal of Rock Mechanics and Mining Sciences. 102 (2018) 57–70. https://doi.org/10.1016/j.ijrmms.2017.12.001.
37. A. Maia da Costa, P. V.M. Costa, A. C.O. Miranda, M. B.R. Goulart, O. D. Udebhulu, N. F.F. Ebecken, R. C. Azevedo, S. M. de Eston, G. de Tomi, A. B. Mendes, J. R. Meneghini, K. Nishimoto, C. Mueller Sampaio, C. Brandão, A. Breda, Experimental salt cavern in offshore ultra-deep water and well design evaluation for CO2 abatement, International Journal of Mining Science and Technology. 29 (2019) 641–656. https://doi.org/10.1016/j.ijmst.2019.05.002.
38. M.B.R. Goulart, P.V.M. da Costa, A.M. da Costa, A.C.O. Miranda, A.B. Mendes, N.F.F. Ebecken, J.R. Meneghini, K. Nishimoto, G.R.S. Assi, Technology readiness assessment of ultra-deep salt caverns for carbon capture and storage in Brazil, International Journal of Greenhouse Gas Control. 99 (2020) 103083. https://doi.org/10.1016/j.ijggc.2020.103083.
39. P.V.M. da Costa, A.M. da Costa, J.R. Meneghini, K. Nishimoto, C.M. Sampaio, G. Assi, E. Malta, M.B.R. Goulart, A. Bergsten, O.D. Udebhulu, R.C. Azevedo, S.M. de Eston, G. de Tomi, N.F.F. Ebecken, L.P. Rosa, A.C.O. Miranda, C. Brandão, A. Breda, Parametric study and geomechanical design of Ultra-deep-water Offshore Salt Caverns for Carbon Capture and Storage in Brazil, International Journal of Rock Mechanics and Mining Sciences. 131 (2020) 104354. https://doi.org/10.1016/j.ijrmms.2020.104354.

40. E.A. Atkinson, P.W. Durling, K. Kublik, C.J. Lister, Qualitative petroleum resource assessment of the Magdalen Basin in the Gulf of St. Lawrence; Quebec, Prince Edward Island, New Brunswick, Nova Scotia, and Newfoundland and Labrador, Geological Survey of Canada, Canada, 2020. https://doi.org/10.4095/321856.
41. A. Lemieux, A. Shkarupin, K. Sharp, Geologic feasibility of underground hydrogen storage in Canada, International Journal of Hydrogen Energy. 45 (2020) 32243–32259. https://doi.org/10.1016/j.ijhydene.2020.08.244.
42. R. Tarkowski, B. Uliasz-Misiak, Towards underground hydrogen storage: A review of barriers, Renewable and Sustainable Energy Reviews. 162 (2022) 112451. https://doi.org/10.1016/j.rser.2022.112451.
43. W. Yan, L. Zou, H. Li, J. Deng, H. Ge, H. Wang, Investigation of casing deformation during hydraulic fracturing in high geo-stress shale gas play, Journal of Petroleum Science and Engineering. 150 (2017) 22–29. https://doi.org/10.1016/j.petrol.2016.11.007.
44. W.-J. Lan, H.-X. Wang, X. Zhang, S.-S. Chen, Sealing properties and structure optimization of packer rubber under high pressure and high temperature, Pet. Sci. 16 (2019) 632–644. https://doi.org/10.1007/s12182-018-0296-0.
45. G. Ghosh, P. Rostron, R. Garg, A. Panday, Hydrogen induced cracking of pipeline and pressure vessel steels: A review, Engineering Fracture Mechanics. 199 (2018) 609–618. https://doi.org/10.1016/j.engfracmech.2018.06.018.
46. J.R. Fekete, J.W. Sowards, R.L. Amaro, Economic impact of applying high strength steels in hydrogen gas pipelines, International Journal of Hydrogen Energy. 40 (2015) 10547–10558. https://doi.org/10.1016/j.ijhydene.2015.06.090.
47. V. Reitenbach, L. Ganzer, D. Albrecht, B. Hagemann, Influence of added hydrogen on underground gas storage: a review of key issues, Environ Earth Sci. 73 (2015) 6927–6937. https://doi.org/10.1007/s12665-015-4176-2.
48. E.R. Ugarte, S. Salehi, A Review on Well Integrity Issues for Underground Hydrogen Storage, Journal of Energy Resources Technology. 144 (2021). https://doi.org/10.1115/1.4052626.
49. R. Kushnir, A. Dayan, A. Ullmann, Temperature and pressure variations within compressed air energy storage caverns, International Journal of Heat and Mass Transfer. 55 (2012) 5616–5630. https://doi.org/10.1016/j.ijheatmasstransfer.2012.05.055.
50. E.W. Lemmon, M.L. Huber, D.G. Friend, C. Paulina, Standardized equation for hydrogen gas densities for fuel consumption applications, SAE Paper. (2006) 01–0434.
51. E.W. Lemmon, I.H. Bell, M.L. Huber, M.O. McLinden, NIST Standard Reference Database 23: Reference Fluid Thermodynamic and Transport Properties-REFPROP, Version 10.0, National Institute of Standards and Technology, Standard Reference Data Program, Gaithersburg. (2018).
52. Y. Zhou, C. Xia, H. Zhao, S. Mei, S. Zhou, An iterative method for evaluating air leakage from unlined compressed air energy storage (CAES) caverns, Renewable Energy. 120 (2018) 434–445. https://doi.org/10.1016/j.renene.2017.12.091.
53. D. Wu, J.G. Wang, B. Hu, S.-Q. Yang, A coupled thermo-hydro-mechanical model for evaluating air leakage from an unlined compressed air energy storage cavern, Renewable Energy. 146 (2020) 907–920. https://doi.org/10.1016/j.renene.2019.07.034.
54. Siemens Energy, Overview of the PEM Silyzer Family, Report, (2020) 4 p. https://assets.new.siemens.com/siemens/assets/api/uuid:abae9c1e48d6d239c06d88e565a25040ed2078dc/version:1524040818/ct-ree-18-047-db-silyzer-300-db-de-en-rz.pdf (accessed June 1, 2022).
55. B. Tang, C. Zhu, M. Xu, T. Chen, S. Hu, Thermal conductivity of sedimentary rocks in the Sichuan basin, Southwest China, Energy Exploration & Exploitation. 37 (2019) 691–720. https://doi.org/10.1177/0144598718804902.
56. M. Labus, K. Labus, Thermal conductivity and diffusivity of fine-grained sedimentary rocks, J Therm Anal Calorim. 132 (2018) 1669–1676. https://doi.org/10.1007/s10973-018-7090-5.

57. F.P. Incropera, D.P. DeWitt, T.L. Bergman, A.S. Lavine, Fundamentals of heat and mass transfer, Wiley New York, 1996.
58. J. Wang, L. Ma, K. Lu, S. Miao, D. Wang, J. Wang, Current research and development trend of compressed air energy storage, Systems Science & Control Engineering. 5 (2017) 434–448. https://doi.org/10.1080/21642583.2017.1377645.
59. X. Zhang, Y. Xu, X. Zhou, Y. Zhang, W. Li, Z. Zuo, H. Guo, Y. Huang, H. Chen, A near-isothermal expander for isothermal compressed air energy storage system, Applied Energy. 225 (2018) 955–964. https://doi.org/10.1016/j.apenergy.2018.04.055.
60. B. Bollinger, Demonstration of Isothermal Compressed Air Energy Storage to Support Renewable Energy Production, Sustainx, Incorporated, Seabrook, NH (United States), 2015. https://doi.org/10.2172/1178542.